On the Control and Effect of Water Content during the Electrodeposition of Ni Nanostructures from Deep Eutectic Solvents

El Amine Mernissi Cherigui,*,† Kadir Sentosun,‡ Mesfin Haile Mamme,† Monika Lukaczynska,† Herman Terryn,† Sara Bals,‡ and Jon Ustarroz*,†

†*Research Group Electrochemical and Surface Engineering (SURF), Vrije Universiteit Brussel, Pleinlaan 2, 1050 Brussels, Belgium*

‡*Electron Microscopy for Materials Science (EMAT), University of Antwerp, Groenenborgerlaan 171, B-2020 Antwerp, Belgium*

E-mail: el.amine.mernissi.cherigui@vub.be; jon.ustarroz@vub.be

Abstract

The electrodeposition of nickel nanostructures on glassy carbon was investigated in 1:2 choline chloride urea (1:2 ChCl-U) deep eutectic solvent (DES) containing different amounts of water. By combining electrochemical techniques, with ex-situ FE-SEM, HAADF-STEM and EDX, the effect of water content on the electrochemical processes occurring during nickel deposition was better understood. At highly negative potentials and depending on water content, Ni growth is halted due to water splitting and the formation of a mixed layer of $Ni/NiO_x(OH)_{2(1-x)(ads)}$. Moreover, under certain conditions, the DES components can also be (electro)chemically reduced at the electrode surface, blocking further 3D growth of the Ni NPs. Hence, a 2D crystalline Ni containing network can be formed in the inter-particle region.

Introduction

In the past few years, the electrochemical synthesis of highly electroactive supported nanostructures has drawn big interest. By tuning the shape, size and chemical composition, these nanomaterials are widely applicable for a broad range of (electro)catalytic applications.[1] Using electrodeposition to synthesize nanostructres has several advantages, especially the ability to obtain nanomaterials with great electrocatalytic activity.[1,2] Aqueous solutions were traditionally used to produce nanoparticles involving different buffers and additives in order to control the electrodeposition processes, in particular for nickel nanostructures, where highly negative potentials are needed.[3–7] The electrodeposition of Ni-based nanostructures on carbon substrates, from aqueous media, is performed using different buffers, such as sulfates,[8,9] phosphates,[7] and acetates.[10–12] However, the use of these electrolytes has several limitations. On the one hand, the deposition of nickel can be performed only at highly negative potentials, and this leads to a local increase in pH due to the reduction of protons and water.[3,4,8] Hence, without controlling the pH, an uncontrollable precipitation of nickel hydroxides will occur, making the reproducibility of the deposition process complicated. Therefore, the use of an adequate buffer is of great importance the deposition of Ni-based nanostructures from aqueous electrolytes.[13] On the other hand, the nanostructures deposited from aqueous baths are often too large and exhibit a broad size distribution due to the low viscosity and high conductivity of these electrolytes.[7–9] Since a homogeneous distribution of small nanoparticles is a critical factor to obtain good electrocatalytic activity, the wide distribution of large Ni structures obtained from aqueous solvents may display a poor activity. Hence, the electrochemical baths require the use of additives to control the deposition process in addition to buffers to control the pH.[13] In recent work, a solution of KCl with H_3BO_3 as buffer and HCl was used in order to control the pH and a homogeneous distribution of small nickel nanoparticles was obtained for very short deposition times.[5,6] Despite this improvement, the presence of hydrogen evolution and the need for using buffered solutions and additives make the deposition of nickel nanostructures from aqueous electrolytes challenging.

In this context, deep eutectic solvents (DESs) have emerged in recent years as a new generation of non-aqueous and cost-effective electrolytes. They offer plenty of advantages compared to traditional aqueous electrolytes or to highly expensive room temperature ionic liquids (RTILs).[14,15] For these reasons, the number of publications on electrodeposition from DES is spectacularly increasing, notably for nickel.[16–34] The electrodeposition from these non-aqueous baths have proven successful to obtain nickel coatings,[18–20,34] nickel-based alloys[21,22,24,25,27,28,35] and nanostructured nickel films for corrosion resistance.[29,30] Similarly, DES were also used for the synthesis of a multitude of nanostructures (Pd,[36] Au,[37] ...), due to the capability of these solvents to slow down the electrochemical processes, thus, having a better control of the deposition of nanostructures.[15] Likewise, DESs are especially interesting because of their ability to stabilize nanoclusters and to facilitate nanoparticle self-assembly without the need for additives and stabilizing agents.[36] Both the halide salt and the hydrogen bond donor (HBD) present in the DES, are expected to influence the shape-controlled synthesis of nanomaterials.[38] Moreover, the unavoidable presence of water, due to the hygroscopicity of these media, makes the deposition processes more complex. In our previous work,[39] we showed that the electrodeposition of nickel nanoparticles (NPs) at a sufficiently negative potential results into the electrocatalytic hydrolysis of residual water in the DES, which leads to the formation of a mixed layer of $Ni/Ni(OH)_{2(ads)}$. A self-limiting growth mechanism was proposed to explain the deposition quenching and the aggregation of nickel nanostructures. A similar mechanism was observed previously from aqueous electrolytes.[40,41] More recently, Palomar-Pardav et al. adapted their analytical model for 3D nucleation and diffusion limited growth taking into account the residual water reduction on the growing surfaces of the Ni NPs.[32] Sebastian et al. studied the electrodeposition of Ni NPs on GC and Pt-based substrates.[33] Similar results to our previous findings[39] on GC were obtained and deeply discussed in their work. Interestingly, small triangular arrays were obtained on Pt(111) at sufficiently low applied overpotential, emphasizing a surface sensitivity of the nucleation and growth mechanisms in DES.[33]

By adding water to the DES, its physico-chemical behaviour is remarkably different due to the change of the intermolecular interactions between the DES constituents.[42–47] Some studies showed that the viscosity and the melting temperature decrease when the water content increases.[46,48,49] To the best of our knowledge, only few studies have focused on the effect of water content on the electrochemical behaviour of DES[44,50,51], as well as on the electrodeposition of nanomaterials.[52] On the one hand, water content has been proven essential to control the electrochemical properties of the DES. In fact, the presence of small amounts of water (up to 6 wt %), has shown to be beneficial for obtaining more uniform and compact Ni coatings.[51] On the other hand, the shape and structure of electrochemically synthesized noble gold nanocrystals could be tuned by changing water content in DES.[52] Hence, the ability of understanding the effect of water and controlling its amount is essential to tune the chemical nature of the electrodeposited nanomaterials from DES, thereby obtaining highly electroactive Ni NPs for a wide range of applications.

Experimental

The 1:2 choline chloride - urea (1:2 ChCl-U) DES, commonly named Reline, was prepared by mixing choline chloride (VWR, hight purity) and urea (ACROS ORGANICS, >99%). In this work, different procedures were used in order to obtain eutectic mixtures with different amounts of water. For dry conditions, choline chloride was recrystallized in absolute ethanol, followed by 12 hours vacuum drying at 80^{o}C. Urea was only dried under vacuum at 80^{o}C for 12 hours. The salts were mixed and heated at 80^{o}C for 24 hours in a glove-box under argon atmosphere in order to obtain the driest DES. For other conditions, i.e. the mixtures containing residual or added water, the salts were used as received. The 1:2 ChCl-U mixture was heated at 80^{o}C in the fume hood for 1 hour under constant pressure of nitrogen. For the dry DES and the one containing residual water, an anhydrous $NiCl_2$ was used in order to obtain a solution containing 10 mM of nickel. For the mixtures with added water, $NiCl_2.6H_2O$

was used. When the nickel salt was completely dissolved, the solution was transferred to the electrochemical cell and kept at 60^oC. An aqueous solution of $NiCl_2.6H_2O$ and NaCl was prepared and added to the DES mixtures in order to obtain different solvents containing 1 $v\%$, 2 $v\%$, 6 $v\%$ and 10 $v\%$ of water, while maintaining the same concentrations of nickel and chloride anions. NaCl was used in order to maintain the same concentration of chloride in the solution. In fact, the Cl/Ni molar ratio could affect the speciation of Ni in the DES.[29] Water quantity was controlled before each experiment using a Metrohm Karl Fischer coulometer. The exact amount of water present in each experiment is reported in $wt\%$ throughout this paper. The calculated values of the molarity (M) and the molar percentages ($mol\%$) of water are reported in Table 1 for the Figures 1, 4, 5, and 7, and in the Supporting Information for the other Figures of the manuscript. Throughout this manuscript, the maximum content of H_2O was kept at 8 $wt\%$ in order to keep the DES integrity. In fact, very high amounts of water will lead to the breakage of ChCl-U interactions due to the complete solvation of the DES components by water molecules.[38,42–44] The electrochemical measurements were performed in an electrochemical cell with a three-electrode system, consisting of a silver wire quasi reference electrode (Ag QRE), a platinum counter electrode and a glassy carbon (GC) disk (6 mm diameter) as working electrode. All the potentials mentioned throughout the manuscript refer to Ag QRE. The potential of this reference electrode is known to be stable in this type of mixtures with high concentration of chlorides.[17]

Table 1: Water content for the experiments showed in Figures 1, 4, 5, and 7, in added $v\%$, $wt\%$ obtained by Karl Fischer measurements, $mol\%$ and molarity (mol/L).

Added water in $v\%$	$wt\%$ (karl Fischer)	$mol\%$	C_{water}(mol/L)
0 (glove-box)	0.06	0.29	0.04
0 (fume hood)	0.55	2.61	0.36
1	1.20	5.11	0.78
2	1.80	7.48	1.17
6	3.96	15.40	2.56
10	5.93	21.78	3.84

Prior to use, the GC working electrodes were polished with 0.3 μm alumina paste, son-

icated twice for 5 min in Milli-Q water and absolute ethanol. For the TEM experiments, Carbon coated TEM grids (CCTGs) were used as working electrodes without any preliminary treatment. More details on the use of CCTGs can be found in previous works.[39,53,54] Before characterization of the nickel deposit, the working electrodes were cleaned with water and ethanol to remove the residual solvent. For the sample prepared in the glove-box, dimethyl carbonate and ethanol were used for the cleaning. The samples were then transferred to the microscope using a vacuum transfer holder to prevent contact with air. It is important to mention that prior to all the depositions reported in this manuscript, an electrochemical pretreatment of the electrode was performed for 180 s at $E = +0.7$ V in order to avoid spontaneous nickel deposition.

The electrochemical experiments were performed by a computer controlled Autolab PGSTAT302. Signal imposing and data acquisition were carried out by NOVA 1.11 software. Scanning electron imaging was handled by a JEOL JSM-7100F field emission scanning electron microscope (FE-SEM), operated at acceleration voltages of 15 kV. High angle annular dark field scanning transmission electron microscopy (HAADF-STEM) images were acquired using an aberration corrected electron microscope (cubed FEI Titan 60300), operated at 300 kV. Energy-dispersive X-ray spectroscopy (EDX) maps were acquired in the transmission electron microscope using a ChemiSTEM system whereas the analysis was performed using the Bruker ESPRIT software.

Results and discussion

Electrochemical Measurements

Figure 1a shows cyclic voltammograms (CVs) recorded on GC from 1:2 ChCl-U containing different amounts of water. The molarity (M) and molar ($mol\%$) percentages of water for all these experiments are reported in Table 1. The CV recorded in dry conditions (0.06 $wt\%$ of water) from the glove-box (Figure 1a, black curve) shows two anodic responses (O_2) and

(O_3) with peak potentials at $E = 0.0$ V, and $E = +0.31$ V, respectively. It must be noted that the assignment of potential at maximum current for (O_2) is approximative due to the substantial broadness of the wave. When the CV is recorded in normal conditions (0.55 $wt\%$ of water) under the fume hood (Figure 1a, grey curve), the anodic peak O_3 shifts to a less positive potential, with peak potential at $E = +0.27$ V, and the charge $Q(O_3)$ slightly increases. When water is added up to 1.2 and 1.8 $wt\%$, respectively, the charge $Q(O_3)$ decreases and $Q(O_2)$ increases (Figure 1a ,green and orange curves). This trend is more predominant when higher amount of water is added, i.e. 3.96 and 5.93 $wt\%$, respectively. Moreover, the peak O_3 becomes broader, while O_2 is sharper (Figure 1a, purple and blue curves). The cathodic sweeps between $E = -0.5$ V and $E = -1.1$ V of the different CVs are shown in Figure 1b. The onsets of the cathodic waves are shown in the inset of Figure 1b. For the driest condition, the cathodic wave R_1 has an onset at $E = -0.80$ V (black curve). Surprisingly, the addition of small amounts of water implies a shift of the onset towards more negative potentials of the cathodic wave (grey and green curve). However, when more water is added, the onset shifts to less negative potentials, especially for larger amounts of water, i.e. 3.96 and 5.95 $wt\%$ (purple and blue curve, respectively). In the case of 3.96 $wt\%$ of water, two cathodic waves, R_1 and R_2, are present within the potential window of the experiment (purple curve), while for 5.95 $wt\%$, a third one (R_3) is also present at highly negative potentials (blue curve). Since the first scan of the CVs depends always on the pretreatment of the bare electrode surface. We believe that presenting the 3^{rd} scan of the CVs is important since the surface is more homogeneous. Figure S1 in the Supporting Information shows the 3^{rd} scan of the CVs shown in Figure1. Similar trends concerning the variation of the electrochemical responses as a function of water content are observed . It is important to mention that all the onsets of the cathodic responses are more negative for the first scan. This is due to the extra overpotential needed for the electrochemical reduction of nickel on bare carbon electrode (1^{st} scan) compared to an electrode containing already some nickel at its surface (3^{rd} scan).

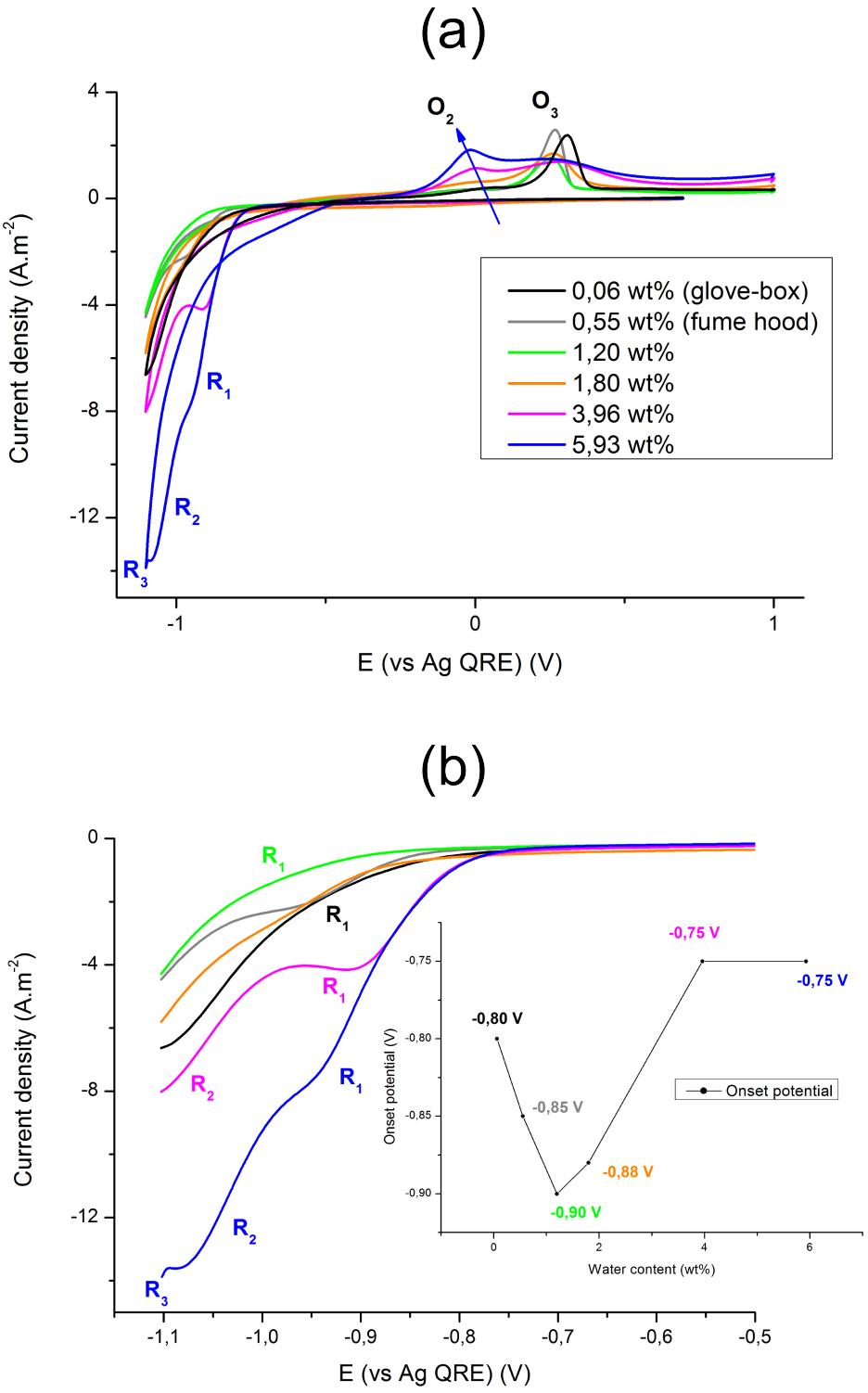

Figure 1: (a) Cyclic voltammograms (1^{st} scan) of 1:2 ChCl-U DES containing 10mM of $NiCl_2$ and recorded on GC in dry conditions from the glove-box (0.06 $wt\%$, black curve), or recorded in normal conditions under the fume hood and containing 0.55 $wt\%$ (grey curve), 1.20 $wt\%$ (green curve), 1.80 $wt\%$ (orange curve), or 3.96 $wt\%$ (purple curve) or 5.93 $wt\%$ (blue curve). (b) Cathodic sweeps between $E = -0.5$ V and $E = -1.1$ V corresponding to the CVs of (a). $\nu = 50$ mV/s. T = $60^{o}C$.

In our previous study,[39] a direct correlation between the processes (R_1) and (O_3) was shown, assigned to the reduction of Ni^{2+} and the stripping of metallic Ni, respectively (eq. 1 and 2). A first tentative assignment of the process (R_2) was made to the electrolysis of water on the deposited nickel nanoparticles. Moreover, the wave (R_3) was attributed to a cathodic breakdown of the DES that is catalysed by the Ni NPs deposited beforehand on the surface of the electrode.[16–19,39]

$$Ni^{2+} + 2e^- \rightarrow Ni \tag{1}$$

$$Ni \rightarrow Ni^{2+} + 2e^- \tag{2}$$

A detailed analysis of the voltammetric peaks can give important information of the processes occurring during Ni deposition in such complex DES-Water mixtures. CVs were recorded on GC and Ni electrodes from blank DES (without nickel salt) containing different amounts of water. Figure 2a shows the cathodic sweep of the CV (1^{st} scan) recorded on a GC electrode. On the one hand, increasing the amount of water leads to an enhancement of the current of two cathodic processes, R'$_1$ and R'$_2$, with onsets at $E = +0.09$ V and $E = -0.23$ V, respectively. These onsets correspond to the DES containing 8.00 $wt\%$ (blue curve). On the other hand, the onset of the process R'$_3$, i.e. the cathodic breakdown of DES, seems not to be dramatically affected by this range of water content. Concerning the waves R'$_1$ and R'$_2$, we believe that they correspond to the reductive adsorption on the surface of the electrode of choline ($C_5H_{14}NO^+$ or Ch^+) and water, respectively. Figure S2a shows the 3^{rd} scan of the CVs shown in Figure2a. A similar trend is observed in 3^{rd} scan compared to the first one.

Similarly, the cathodic sweep of the CV (1^{st} scan) recorded on Ni electrode are shown in Figure 2b. The curves exhibit three cathodic waves and are coded R"$_1$, R"$_2$ and R"$_3$, respectively. It is important to notice that increasing slightly the amount of water (up to 0.46 $wt\%$, grey curve) leads to a slight enlargement of the potential window. The latter decreases when more water is added (1.09 and 1.91 $wt\%$, green and orange curves). Increasing largely

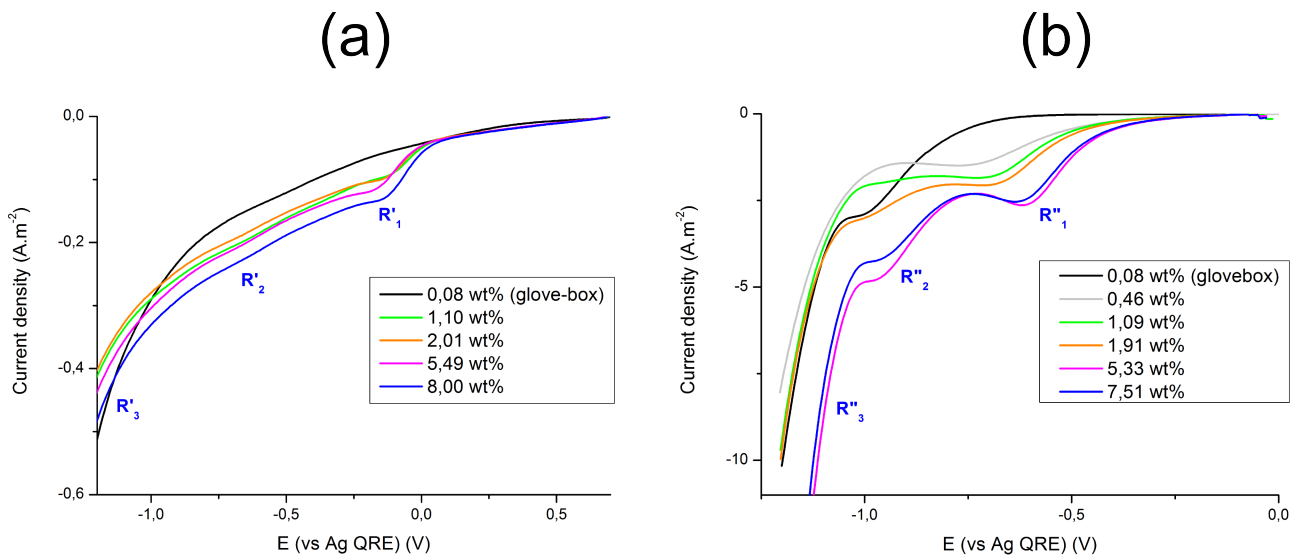

Figure 2: Cathodic sweep of the cyclic voltammograms (1^{st} scan), recorded on (a) GC or (b) Ni electrode, of 1:2 ChCl-U: containing different amounts of water. ν = 50 mV/s. T = 60^oC.

the amount of water (up to 7.51 $wt\%$) enhances the currents of the waves R"$_1$ (onset at E = -0.18 V for the blue curve) and R"$_2$ (onset at $E = -0.67$ V for the blue curve) and decreases drastically the potential window (purple and blue curves). First tentative assignment of these two processes could be to the adsorption of water on the polycrystalline nickel electrode[3,55] (eq. 3). The presence of nickel hydrides could explain the shift of the peak O_3 toward more negative potentials, as shown in Figure 1a.

$$Ni + H_2O + e^- \rightarrow Ni - H_{ads} + OH^- \tag{3}$$

Concerning the cathodic breakdown (R"$_3$), an interesting behaviour is observed. For the experiment performed in the glove-box, the onset of this cathodic response is recorded at E = -1.03 V. This process corresponds to the cathodic decomposition of choline cations[56] (eq. 4).

$$C_5H_{14}NO^+ + e^- \rightarrow C_3H_9N + .C_2H_5O \; or \; C_4H_{11}NO + .CH_3 \tag{4}$$

We believe that the electrolysis of residual water is likely happening simultaneously(eq. 5).

$$2H_2O + 2e^- \rightarrow H_2 + 2OH^- \tag{5}$$

Adding a small amount of water to the solvent leads firstly to a shift of the onset of R"$_3$ towards more negative potentials $E = -1.08$ V (0.55 $wt\%$, grey curve). Thus, the potential window of the DES on Ni electrode increases. For higher amount of water, the onset shifts toward more positive potentials (1.09 and 1.91 $wt\%$, green and orange curves, respectively). Moreover, adding larger amounts of water (5.33 and 7.51 $wt\%$, purple and blue curves, respectively) leads to a bigger positive shift of the onset ($E = -0.97$ V for the blue curve). Similar trend is shown in the 3^{rd} scan of the CVs (Figure S2b in the Supporting Information). In this case, such amount of water (5.33 $wt\%$ and 7.51 $wt\%$) leads to the disruption of the DES integrity.[51] Therefore, the measured current is caused by the water electrolysis, like in aqueous solutions, since it occurs at more positive potentials than the reduction of Ch^+. In addition, we believe that the presence of a large excess of OH^-, generated by water electrolysis, at the interface could lead to a chemical breakdown of the choline cations, i.e. Hoffman elimination (eq. 6).[56] An electrochemical pathway in the presence of hydroxide anions is also plausible (eq. 7) and may lead to the formation of some by-product similar to the one of eq. 4 and 6.

$$C_5H_{14}NO^+ + OH^- \rightarrow C_3H_9N + C_2H_4O + H_2O \tag{6}$$

$$C_5H_{14}NO^+ + 1e^- + OH^- \rightarrow organic\,by-products \tag{7}$$

To elucidate the anodic processes occurring on Ni electrode, the recorded CVs for different water content are shown in Figure 3. Adding water to the mixture leads to the emergence of the anodic response O_2, with wave potential at $E = 0$ V. For higher amounts of water, another broad anodic process is present and coded O'$_2$, with wave potential at $E = -0.19$

V (purple and blue curves). According to previous studies from alkaline aqueous solutions, these different anodic processes could be assigned to different oxidation processes. On the one hand, the anodic process O_2 could be assigned to the oxidative desorption of hydrogen.[57–60] This hydrogen could be adsorbed at the surface of the electrode[57,58] but also absorbed in the bulk nickel phase.[59–61] On the other hand, O'_2 could be attributed to the formation of $Ni(OH)_{(ads)}$ and $Ni(OH)_{2(ads)}$.[55,62,63] Since the potential was swept to highly negative values, an excess of OH^- is formed, by water electrolysis, at the interface and stabilized by the hydrogen bonds with the DES components. Thus, the assignment of anodic processes in alkaline solutions could be plausible in our case. The cathodic process $R"_1$ and $R"_2$ could be due to the adsorption/absorption of hydrogen on two different phases of Ni, i.e. α-Ni and β-Ni, where the latter is richer in hydrogen than the former. This behavior was previously described in aqueous solutions[3] as well as on DESs.[64] Figure S3 in the Supporting Information shows the 3^{rd} scan of the different CVs. It is important to mention that in the case of hight water content (3.96 and 5.96 $wt\%$, purple and blue curves, respectively), another broad anodic wave O_1 is present at $E = -0.32$ V. Moreover, the intensity of O'_2 increases while the one of O_2 decreases. This behavior is related to the passivation phenomena which is enhanced by the presence of high water content. More explanations will be given further.

To further understand the (electro)chemical processes occurring at different deposition potentials / amounts of water, different electrochemical experiments were undertaken. Depositions were followed by anodic LSV to elucidate the effect of cathodic processes on the subsequent anodic responses.[39] Figure 4a shows several LSVs recorded in dry conditions after deposition at different potentials for 120 s. For a deposition at less negative potential ($E = -0.65$ V, orange curve), the subsequent LSV shows a small O_3 and no O_2. When the depositions are performed at more negative potentials ($E = -0.72$ V, green curve and $E = -0.9$ V, black curve), the recorded LSVs exhibit a big increase of the charge of nickel stripping peak (O_3) and feature the anodic wave O_2, for which, the charge increases for more negative potential (black curve). Likewise, a wide anodic wave O_1 appears for more

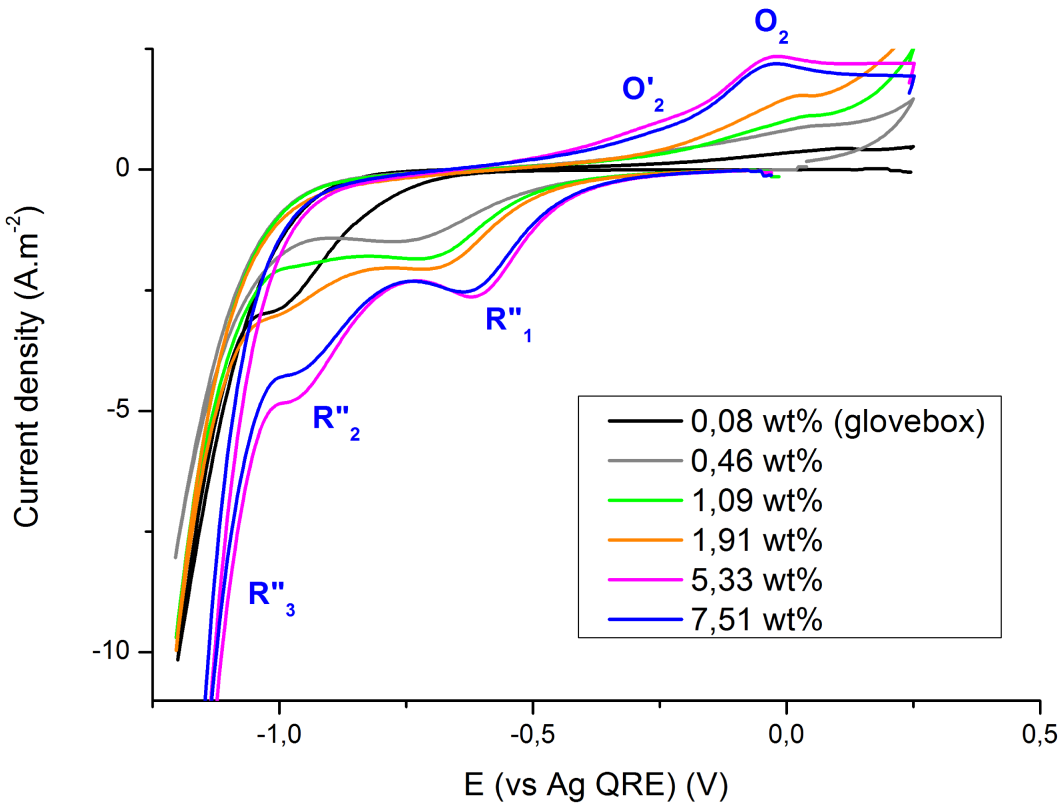

Figure 3: Cyclic voltammograms (1^{st} scan), recorded on Ni electrode, of 1:2 ChCl-U: containing different amounts of water. ν = 50 mV/s. T = 60^oC.

negative potential (black curve). For a deposition at much more negative potential ($E = -1.1$ V, red curve), the anodic responses O_1, O_2 and O_3 vanish almost completely and a new one (O_4) appears. This behaviour was described previously[39], and was assigned to a full passivation or inhibition against Ni stripping, when an anodic LSV is recorded subsequently after a deposition at highly negative potential. Similar experiments were conducted from DES with 10 $v\%$ added water (Figure 4b). In this case, the two anodic processes (O_2) and (O_3) are present in the LSVs recorded after depositions at less negative potentials ($E =$ -0.60 V, grey curve and $E = -0.65$ V, orange curve). When the depositions occur at more negative potential ($E = -0.72$ V, green curve), the charges $Q(O_2)$ and $Q(O_3)$ are higher. Moreover, a broad shoulder O'_3 appears on the stripping wave of metallic nickel. Sebastian et al.[33] showed that the presence of two types of metallic nickel (bulk and embrittled by hydrogen) can give rise to such phenomenon. In fact, this shoulder vanishes and merges within the broadness of O_3 for depositions at more negative potential ($E = -0.8$ V, blue curve). Afterwards, the charge $Q(O_2)$ increases while $Q(O_3)$ decreases ($E = -0.9$ V, black curve). We believe that the presence of nickel hydrides could be the reason of this behaviour as shown in eq. 3.

It is clear from Figures 1 and 4 that both water and the deposition potentials have an effect on the electrochemical processes. In order to clarify the effect of these two parameters, the anodic LSVs for different deposition potentials and water contents are shown in Figure 5. For depositions at $E = -0.90$ V (Figure 5a), the subsequent LSVs show two anodic responses O_2 and O_3. For small amounts of water (up to 1.80 $wt\%$), the anodic wave O_3 is sharp and its charge $Q(O_3)$ is predominant (black, grey, green and orange curves). The presence of higher amounts of water implies an increase of the charge $Q(O_2)$. Moreover, the anodic wave O_3 becomes broader and its charge decreases (purple and blue curves). It is important to notice that all the LSVs show an anodic wave starting around $E = +0.78$ V whose extent is more important for higher amounts of water (purple and blue curves). For depositions at highly negative potential ($E = -1.1$ V, Figure 5b), all the recorded LSVs show the anodic processes

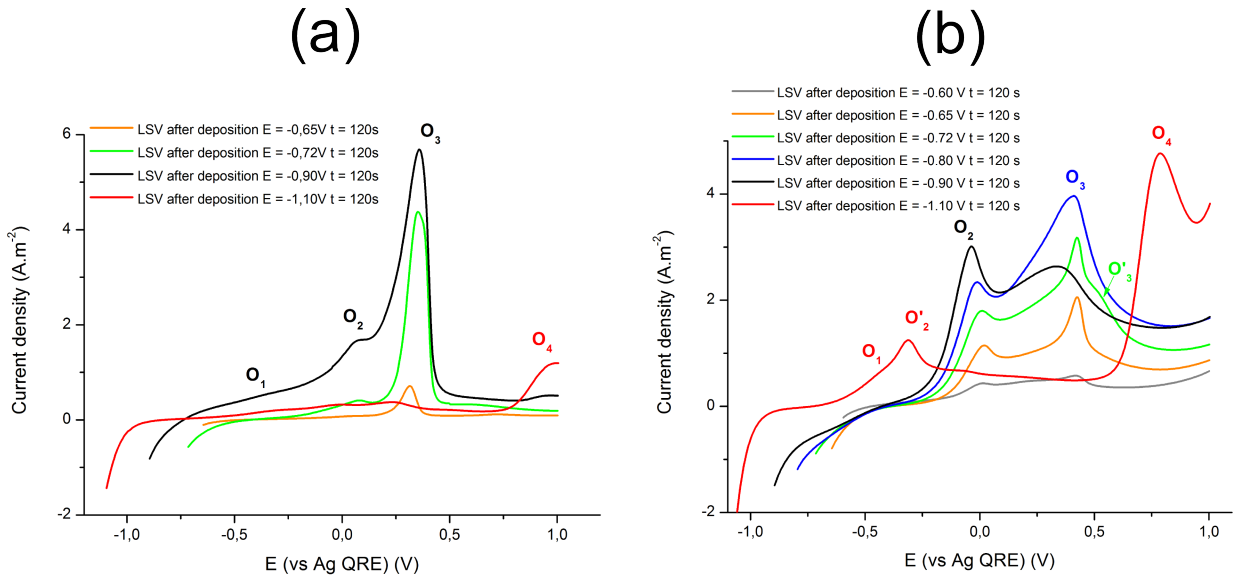

Figure 4: LSV recorded on GC after a potentiostatic deposition of nickel for 120s at $E = -0.6$ V (grey curve), $E = -0.65$ V (orange curves), $E = -0.72$ V (green curves), $E = -0.8$ V (blue curve), $E = -0.9$ V (black curves) and $E = -1.1$ V (red curves) from 1:2 ChCl-U containing (a) 10mM of anhydrous $NiCl_2$ and performed in dry conditions from the glove-box (0.06 $wt\%$) and (b) 10 mM of $NiCl_2$-$6H_2O$ (5.93 $wt\%$). $\nu = 50$ mV/s, T = 60^oC.

O_1 and O'$_2$. For a dry DES (black curve), the charges of these processes are extremely low compared to more wet mixtures. On the one hand, the processes O_1 and O'$_2$ shift to more negative potentials when large amounts of water are added (3.96 and 5.93 $wt\%$) while their charges are slightly affected. On the other hand, the charge $Q(O_4)$ is directly related to the water content in the DES. In all these cases, no Ni stripping occurs.

In order to clarify such inhibition process, the influence of stirring during the electrochemical deposition at highly negative potential was investigated (See the Supporting Information).

All the aforementioned experiments help us to gain a better understanding of the electrochemical behaviour of nickel in a choline chloride urea DES, as well as the effect of water content on the different electrochemical processes. A summary of all the electrochemical processes are show schematically on Figure 6.

According to the LSVs and CVs shown in Figures 2 and 3, the presence of a small amount of water in the DES increases the potential window of the solvent. This slight increase in the

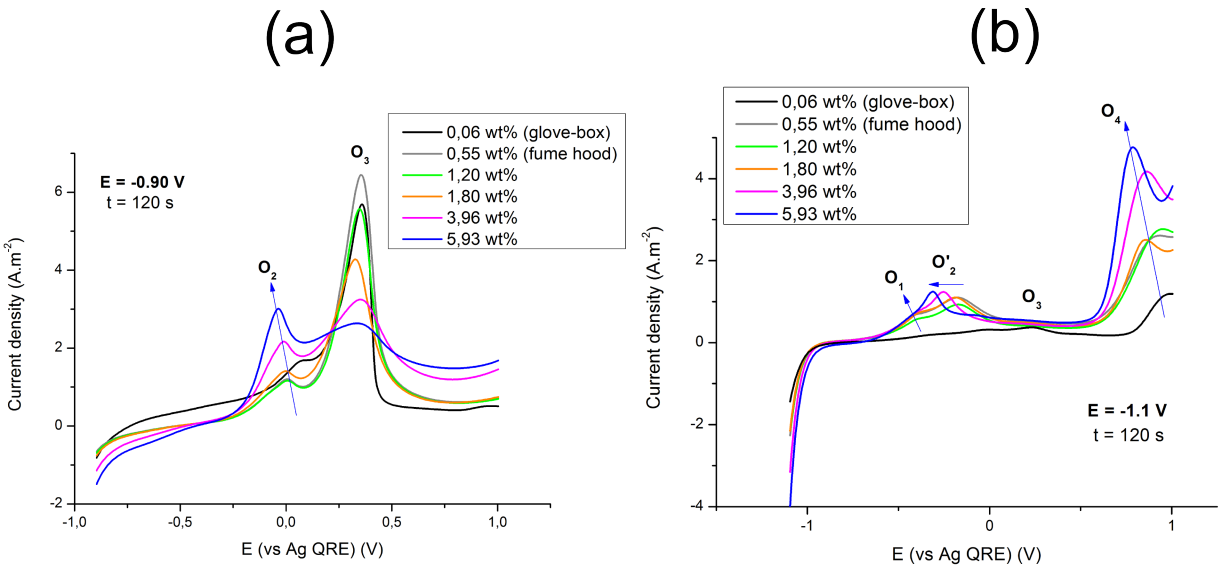

Figure 5: LSV recorded on GC after a potentiostatic deposition of nickel for 120s at (a) $E = -0.9$ V and (b) $E = -1.1$ V from 1:2 ChCl-U: containing 10mM of anhydrous $NiCl_2$ recorded in dry conditions (0.06 $wt\%$) from the glove-box (black curves), or recorded in normal conditions (0.55 $wt\%$) under the fume hood (grey curves); containing 10mM of $NiCl_2$-$6H_2O$ and 1.20 $wt\%$ H_2O (green curves) or 1.80 $wt\%$ H_2O (orange curves) or 3.96 $wt\%$ H_2O (purple curves) or 5.93 $wt\%$ H_2O (blue curves). $\nu = 50$ mV/s, T = 60^oC.

potential window could be due to an inhibition of water splitting and Ch^+ reduction, owing to a strong intermolecular interaction between H_2O molecules and Reline species[42,51]. For larger amounts of water (5.33 $wt\%$ and 7.51 $wt\%$, Figure 2b and 3), the potential window diminishes drastically. In fact, for a such water content, the DES molecules are fully solvated in a similar way as in an aqueous solution. Hence, the intermolecular interactions of the DES are weakened[44,50,51], leading to an enhanced reduction of the choline cations and the water molecules at the electrode.

In the presence of nickel in the DES (Figure 1), adding small amounts of water (up to 1.20 textitwt%) leads to a negative shift of the onset for nickel reduction, compared to a drier DES (0.08 $wt\%$). For larger water contents (3.96 and 5.93 $wt\%$ H_2O), the onset of nickel reduction is shifted to more positive potentials. The latter positive shift can be related to an increase of conductivity and decrease of viscosity of the solvent, when the water is added to the DES. However, the negative shift occurring for smaller amounts of added

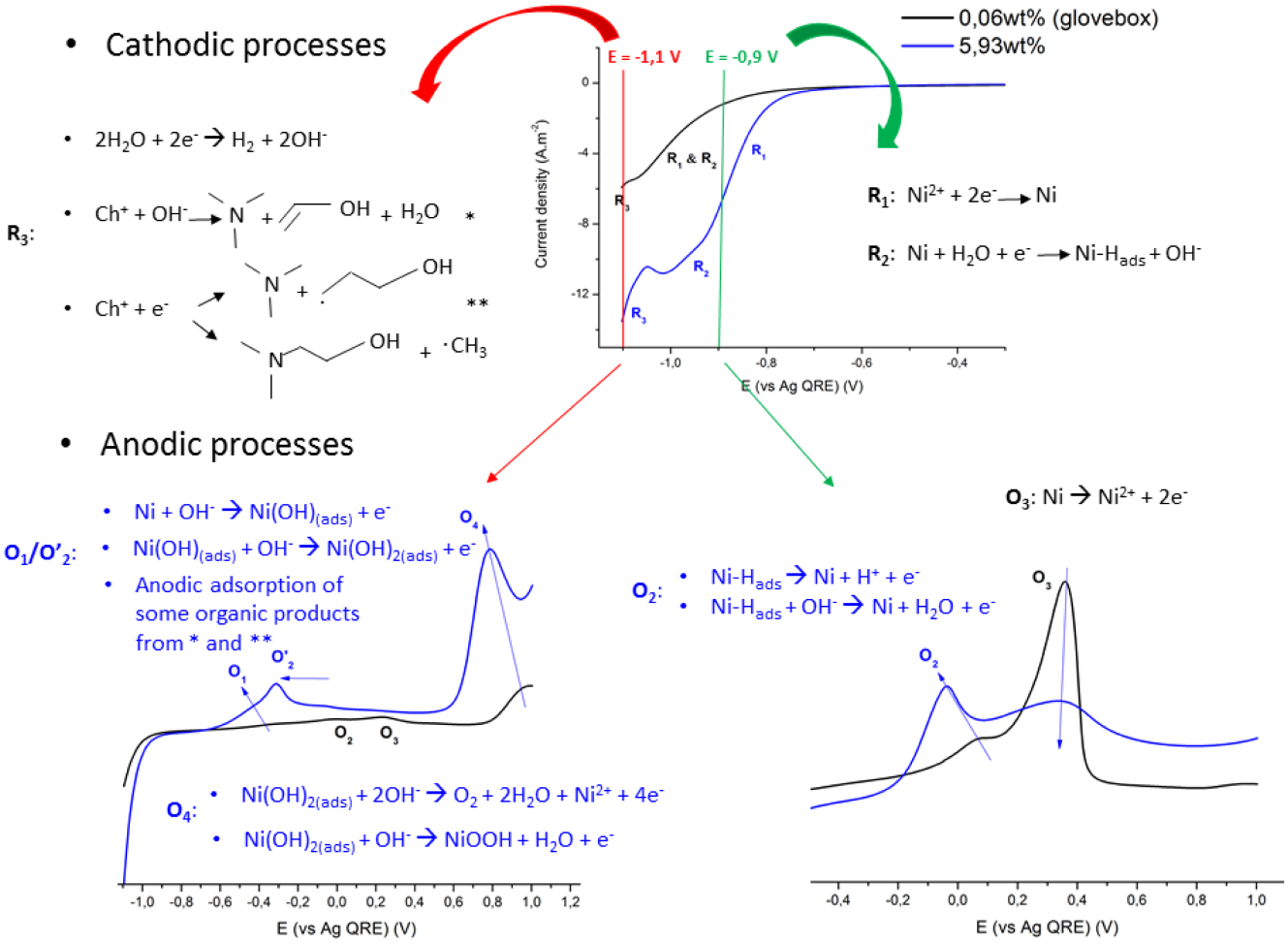

Figure 6: Summary of the different cathodic and anodic processes occurring during Ni electrodeposition from 1:2 ChCl-U DES

water cannot be explained straightforwardly. Since water, urea and chloride anions are most likely involved in the speciation of Ni in the DES, adding a small amount of water could be responsible of a change of this speciation leading to more stable Ni complexes (more difficult to be reduced). In fact, adding small quantities of water may as well induce a strengthening of the interactions between the different DES component and the Ni complexes, whereas adding large amounts of water could lead to the full solvation of the DES components, and hence to the loss of the solvent integrity.

These assumptions could be checked by studying the double layer composition at the electrode, taking into account the applied potential, water content and nickel concentration. These studies are ongoing in our group by using atomistic molecular dynamics simulations. We have previously used the same approach to explore the inter-molecular interactions between the DES components, as well as the distribution and electrosorption of water at the interface. Further details can be found elsewhere.[65]

Concerning the anodic wave O_2, it is clear from Figure 1 that this process is dependent on the amount of water present in the media. Plus, it was observed in the CVs of the blank DES recorded on the Ni electrode (Figure 3). Consequently, this response could be assigned to the oxidation of absorbed[59,60] and/or adsorbed hydrogen[55,57,58] (eq. 8).

$$Ni - H_{(ads)} \rightarrow Ni + H^+ + e^- \tag{8}$$

In the presence of an excess of OH^-, the oxidation of the adsorbed hydrogen can follow the reaction of eq. 9, for alkaline media.[55] The concentration of OH^- at the interface is depending on the amount of water present in the solvent but also on the applied potential. And since the charge $Q(O_2)$ depends also on the water content (see Figure 1a and 5a) and on the applied potential (see Figure 4b), we believe that eq. 9 is the most conceivable for the process O_2.

$$Ni - H_{(ads)} + OH^- \rightarrow Ni + H_2O + e^- \tag{9}$$

As evinced previously, the anodic responses O_1 and O'_2 are surface processes dependent on the applied potentials (Figure 5b and 3) and can be avoidable by performing the highly negative depositions under stirring conditions (Figure S4). Moreover, the charge of this anodic phenomenon is dependent on the amount of Ni NPs present on the electrode surface. In fact, a few amount of Ni nanostructures at the surface leads to a small charge $Q(O_1)$, as shown in Figure 10(a) (see the section: TEM characterization) and 5b (black curve). They could be related to the anodic adsorption of OH^- groups (produced during water splitting as shown in eq. 5) on the surface of Ni, preventing its anodic stripping[39] (eq. 9 and 10). Another conceivable explanation for these processes is the oxidation of some by-products resulting from the reduction of choline cations at highly negative potentials (eq. 4 and 6). The latter hypothesis agrees well with the fact that the whole electrode (Ni NPs and carbon) are passivated after a deposition at highly negative potential followed by immediate anodic polarization.[39] We believe that a mixed $Ni(OH)_{2(ads)}$ / organic layer might be formed at the surface preventing Ni stripping and further Ni^{2+} reduction.[39]

$$Ni + OH^- \rightarrow Ni(OH)_{(ads)} + e^- \tag{10}$$

$$Ni(OH)_{(ads)} + OH^- \rightarrow Ni(OH)_{2(ads)} + e^- \tag{11}$$

Finally, the anodic response O_4 was already assigned to an oxygen evolution reaction involving an oxidative electrodissolution of $Ni(OH)_2$ formed at highly negative potentials[39] (eq. 12).

$$Ni(OH)_{2(ads)} + 2OH^- \rightarrow O_2 + 2H_2O + Ni^{2+} + 4e^- \tag{12}$$

A partial oxidation of the $Ni(OH)_{2(ads)}$ to form NiOOH is also possible (eq. 13).

$$Ni(OH)_{2(ads)} + OH^- \rightarrow NiOOH + H_2O + e^- \tag{13}$$

This mechanism seems to be plausible since this anodic response increases with the

water content in the mixture, i.e. more OH^- is produced at highly negative potentials. It is interesting to see that this anodic response is also present in the LSV recorded after a deposition at $E = -1.1$ V under forced-convective conditions (Figure S4b). Thus, an incorporation of $Ni(OH)_{2(ads)}$ in the deposit is believable.

FE-SEM characterization

The complexity of the electrochemical processes may allow different growth regimes depending on the water content and applied potential. In this way, representative FE-SEM images of nickel NPs deposited for 120 s at $E = -0.8$ V and at $E = -1.1$ V, from two mixtures containing different amounts of water are shown in Figure 7. Ni nanostructures obtained from a DES containing 10mM of dry $NiCl_2$ and 0.55 $wt\%$ H_2O at $E = -0.8$ V are shown in Figure 7a. A dense and homogeneous distribution of small NPs is obtained. The total charge involved in this process is Q = -97.1 C/m^2. For a DES containing 5.94 $wt\%$ H_2O, slightly larger NPs with a rounded shape are obtained as shown in Figure 7b. The total charge involved in this process is Q = -278.6 C/m^2. The increase of the total charge and the size of the NPs is related to the low overpotential needed for Ni deposition from a DES containing 5.94 $wt\%$ compared to a DES prepared in normal conditions and containing a residual amount of water (see Figure 1b), owing most likely to a decrease of the viscosity and and an increase of the conductivity. Figures 7c and 7d show the nanostructures obtained at $E = -1.1$ V from a DES prepared in normal conditions (0.55 $wt\%$ H_2O) and a DES containing 5.94 $wt\%$. The total charges involved in the depositions are Q = -353.9 C/m^2 and Q = -646.0 C/m^2 respectively. In both cases, a less dense distribution of Ni nanoclusters is obtained. The increase of the total charge and no significant increase of electrodeposited Ni from a DES containing 5.94 $wt\%$ H_2O confirm our previous results, suggesting parallel electrochemical processes, occurring at highly negative potentials and related to the presence of water in the DES. Moreover, the FE-SEM image for a deposition at $E = -1.1$ V from a DES containing 5.94 $wt\%$ H_2O shows some black spots covering the NPs (red circles in

Figure 7d). These dark areas can be easily seen from a lower magnification FESEM image as shown in Figure 7e. We believe that these features can be due to the incorporation of DES reaction products (eq. 4, 6 and 7). Also, longer and more extensive cleaning with water and ethanol was needed for the samples prepared in these conditions.

3. TEM characterization

In the present study, carbon-coated TEM grids were used as electrochemical electrodes. Figures 8a and b show low and high-resolution HAADF-STEM images acquired after deposition at $E = -0.9$ V for 60 s from a dry DES (0.06 $wt\%$ H_2O), respectively. The Ni nanostructures are aggregates of clusters whose size varies between 5 and 20 nm. The difference in HAADF-STEM contrast of the NPs core and the surrounding shell suggests the formation of a core-shell structure.[39] Similar structures are present for depositions performed from DES containing 4.64 $wt\%$ (Figures 8c and d) and 6.74 $wt\%$ H_2O (Figures 8e and f). However, the aggregates seem to be formed by larger and more dense clusters compared to the aggregates obtained from dry conditions (0.06 $wt\%$ H_2O), owing to a decrease of the kinetic viscosity as well as to an increase of the conductivity for higher water content (4.64 $wt\%$ and 6.74 $wt\%$ H_2O).

Selected area electron diffraction (SAED) was performed for the different samples (Figure S5 of the Supporting Information), and both crystalline Ni and NiO are present. These results are in agreement with our previous work that shows that Ni NPs deposited from 1:2 ChCl-U (containing residual amount of water) are made by a crystalline metallic Ni core and a crystalline NiO shell.[39] EDX mapping was performed on Ni NPs electrodepposited from a DES containing 6.74 $wt\%$ H_2O. The core-shell structure was confirmed. In fact, the Ni content is higher at the core, whereas the O is mostly present at the edges (Figures 9(a) and (b)).

Figures 10a and b show a low and high-resolution HAADF-STEM image acquired after deposition at $E = -1.1$ V for 60 s from a dry DES (0.06 $wt\%$ H_2O). The micrographs

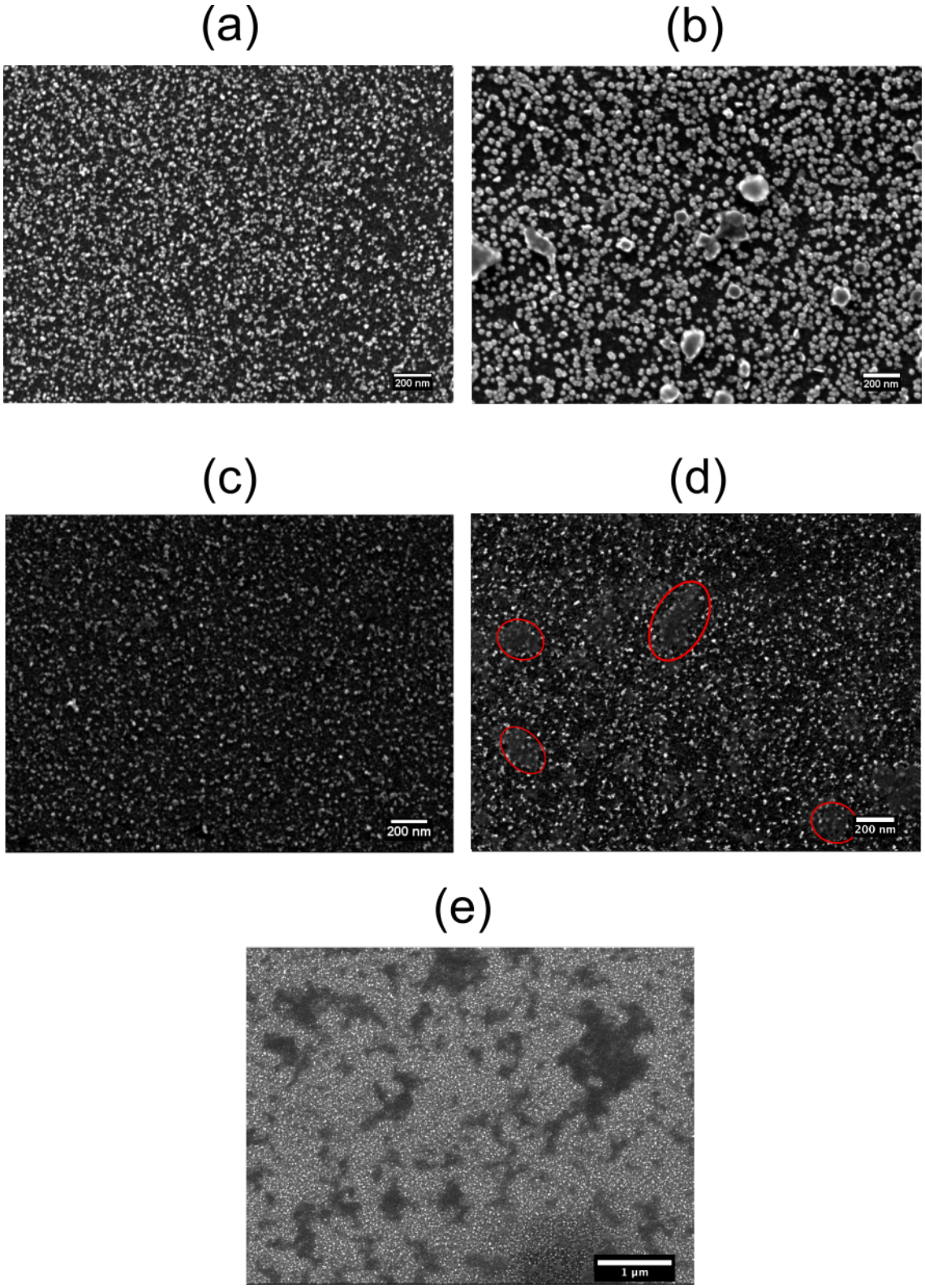

Figure 7: FE-SEM images of the nickel nanostructures deposited on GC for 120 s at (a) and (b) $E = -0.8$ V and at (c) and (d) $E = -1.1$ V from (a) and (c) 1:2 ChCl-U containing 10mM of dry $NiCl_2$ and 0.55 $wt\%$ H_2O, or (b) and (d) and (e) 1:2 ChCl-U containing 10 mM of $NiCl_2$-$6H_2O$ and 5.94 $wt\%$ H_2O. T = 60^oC.

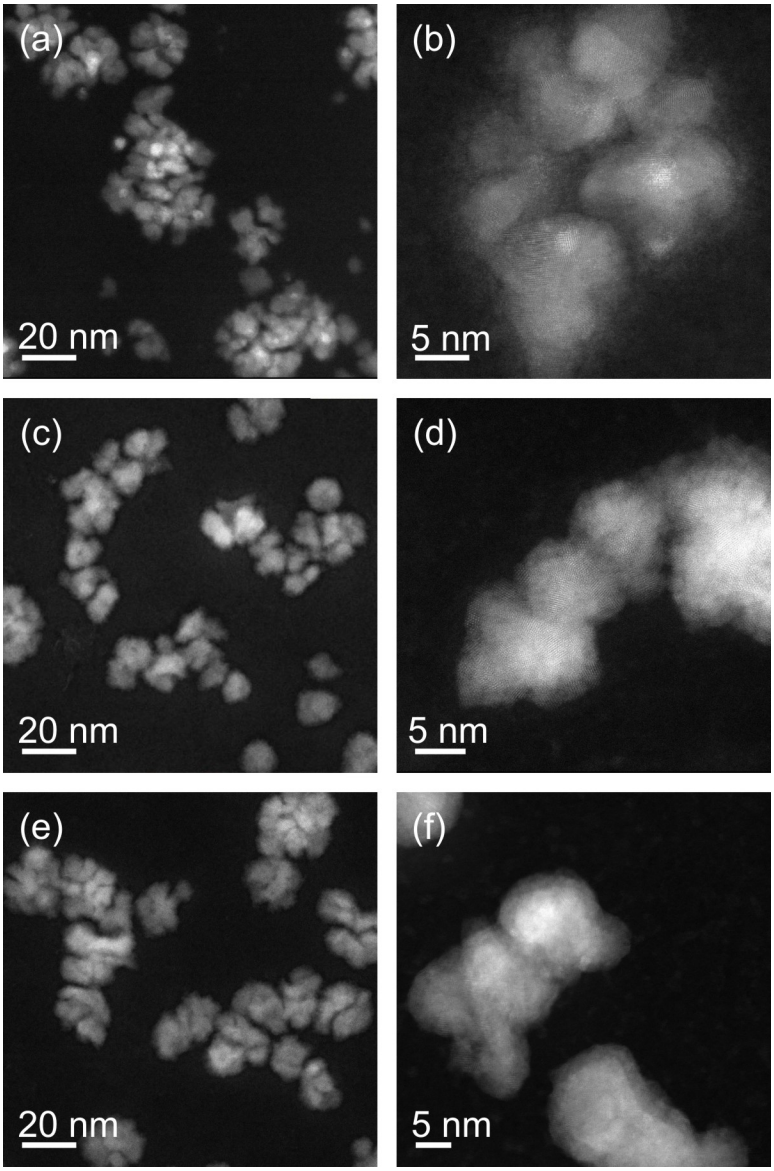

Figure 8: HAADF-STEM micrographs of Ni NPs after deposition for 60 s at $E = -0.9$ V from (a) and (b) a dry DES (glove-box) containing 0.06 $wt\%$ H_2O and a DES containing 10 mM of $NiCl_2$-$6H_2O$ and (c) and (d) 4.64 $wt\%$ H_2O (6 $v\%$) and (e) and (f) 6.74 $wt\%$ H_2O (10 $v\%$). T = 60^oC.

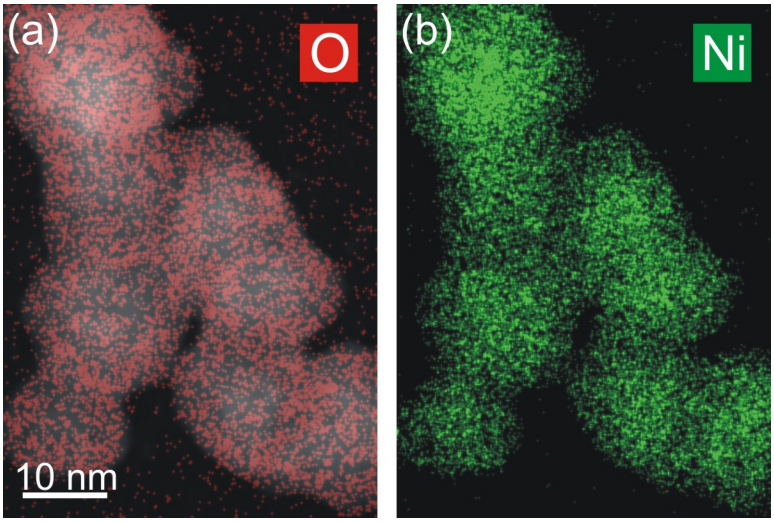

Figure 9: EDX map results for Ni NPs after deposition for 60 s at $E = -0.9$ V from a DES containing 10 mM of $NiCl_2$-$6H_2O$ and 6.74 $wt\%$ H_2O (10 $v\%$). T = 60^oC. (a) The overlay between HAADF image and O map. (b) The overlay between HAADF image and Ni map.

reveal that the NPs consist of agglomerated small crystallites ranging between 3 and 10 nm. For higher water content, i.e 4.64 $wt\%$ H_2O (Figures 10c and d) and 6.74 $wt\%$ H_2O (Figures 10e and f), the deposits consist of a more dense and homogeneous distribution of agglomerates. Compared to the deposition at lower overpotential (Figure 8a), the amount of nickel nanostructures is drastically lower for a deposition at $E = -1.1$ V (Figure 10(a)). At this range of potentials, the electrolysis of water and the decomposition of choline cations are occurring in parallel with the deposition process, quenching the growth. We believe that the formation of $NiO_x(OH)_{2(1-x)}$ is responsible for the growth self-termination, similarly to that reported in aqueous solutions.[5,6,40,41] Furthermore, we believe that the reduction of choline cations could also be responsible for the growth self-termination.

For higher water content (4.64 $wt\%$ and 6.74 $wt\%$ H_2O), and despite the inhibition of growth described before, more Ni nanostructures are present on the surface of the electrode (Figures 10c and 10e) compared to the deposition performed in dry conditions (0.06 $wt\%$ H_2O. Figure 10(a)). This can be due to a lower viscosity for this range of water concentrations, i.e. the products of the side reactions can diffuse away from the surface allowing more nickel to be reduced at the electrode.

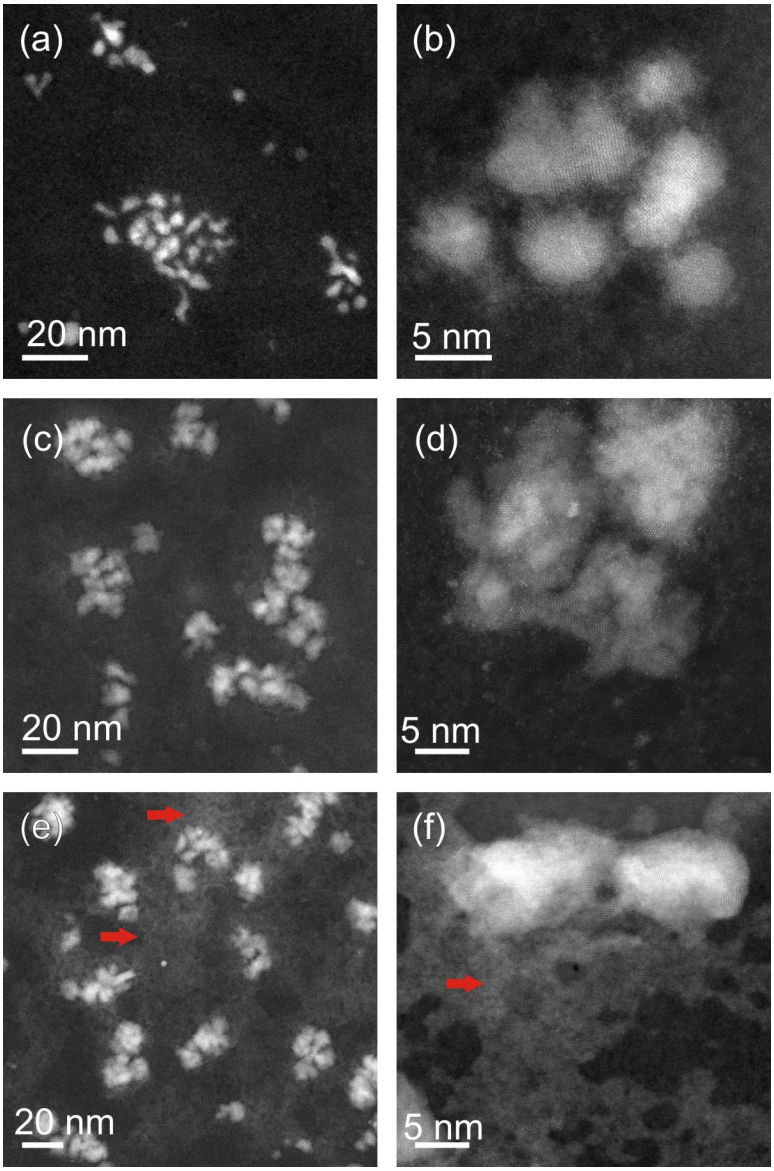

Figure 10: HAADF-STEM micrographs of Ni NPs after deposition for 60 s at $E = -1.1$ V from (a) and (b) a dry DES (glove-box) containing 0.06 $wt\%$ H_2O and a DES containing 10 mM of $NiCl_2$-$6H_2O$ and (c) and (d) 4.64 $wt\%$ H_2O (6 $v\%$) and (e) and (f) 6.74 $wt\%$ H_2O (10 $v\%$). T = 60^oC.

EDX mapping was performed on Ni NPs electrodeposited from a DES containing 6.74 $wt\%$ H_2O. The map clearly shows that oxygen is present homogeneously across the NPs (Figure 11), similarly to our previous work.[39] Surprisingly, a 2D crystalline Ni containing network is formed in the inter-particle region, as depicted with red arrows in the Figures 10e and f. SAED patterns (Figure S6 of the Supporting Information) confirm the presence of both Ni and NiO in a crystalline form.

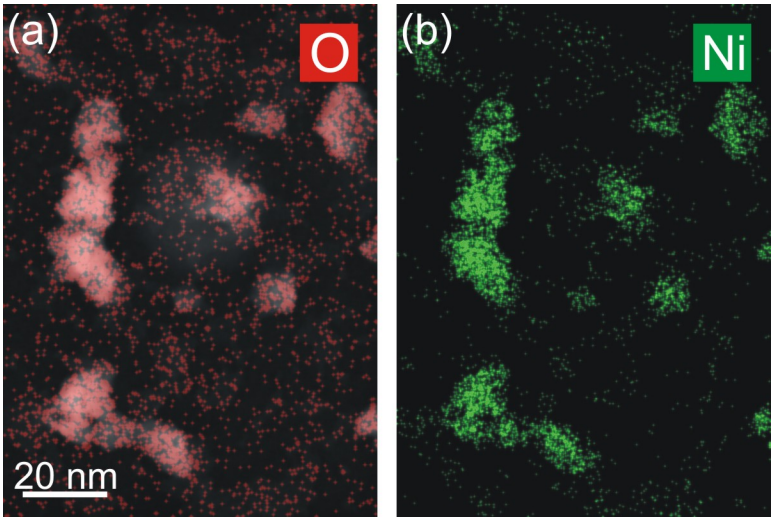

Figure 11: EDX map results for Ni NPs after deposition for 60 s at $E = -1.1$ V from a DES containing 10 mM of $NiCl_2$-$6H_2O$ and 6.74 $wt\%$ H_2O (10 $v\%$). T = 60^oC. (a) The overlay between HAADF image and O map. (b) The overlay between HAADF image and Ni map.

Discussion

The study of the water content effect on the electrodeposition of nickel nanostructures was performed by combining electrochemical experiments with *ex-situ* characterization techniques, such as FE-SEM, HAADF-STEM and EDX.

HAADF-STEM pictures show a more dense distribution of smaller aggregates when the depsoitions are performed at low overpotential ($E = -0.9$ V) from DES containing high water content, as depicted in Figure 8. This can occur for two reasons. First of all, high increase of the water content in DES, induces a decrease of the kinetic viscosity and an

increase of the electrical conductivity. Hence, a higher nucleation rate could be observed for Ni NPs.[51] Secondly, the growth self-termination of the Ni nanostructures by water hydrolysis is predominant when the concentration of water is higher, leading to smaller aggregates.

At highly negative potentials ($E = -1.1$ V), Ni growth is halted due to water splitting and the formation of a mixed layer of $Ni/Ni(OH)_{2(ads)}$.[39] Moreover, for higher water content, the DES components can also be (electro)chemically reduced at the electrode surface, blocking further 3D growth of the Ni NPs (See the black non-conductive spots covering the NPs in Figures 7d and e). Hence, a 2D crystalline Ni containing network can be formed in the inter-particle region, as depicted in Figures 10(e) and (f). Choline cations can be reduced electrochemicaly to form either a trimethylamine and an ethanol radical or dimethylaminoethanol and a methyl radical.[56] Furthermore, the presence of OH^- at highly negative potentials will lead to a chemical decomposition of choline cations via Hoffman elimination reaction, leading to the formation of a trimethylamine, a vinyl alcohol and a molecule of water. Note that a subsequent anodic polarisation has been shown to lead to the passivation of the whole electrode surface against Ni stripping and further Ni reduction.[39] We believe that the anodic processes O_1 and O'_2 are responsible of this phenomenon as shown before in Figures 4b, 5b and S1 b. The formation of a full layer of $Ni(OH)_{2(ads)}$ on the surface of Ni NPs and an (anodic) adsorption of an organic layer on the surface of the electrode could explain the inhibition of Ni stripping and further Ni^{2+} reduction, as depicted in Figure 12.

Understanding the role of added water during the electrochemical deposition and the interaction between DES components and the growing nickel NPs is essential to tune the size, shape and chemical composition of the Ni nanostructures and therefore, producing highly electroactive supported nanoparticles for (electro)catalytic applications. Being able to control the self-limiting growth of metals allows obtaining several interesting nanostructures, such us monoatomic films, high surface-area structures and as presented for the first time in this work, 3D nanostructures connected by a 2D network. These novel nickel nanostructures, composed of distributions of $Ni/NiO_x(OH)_{2(1-x)}$ NPs linked by a 2D crystalline Ni network

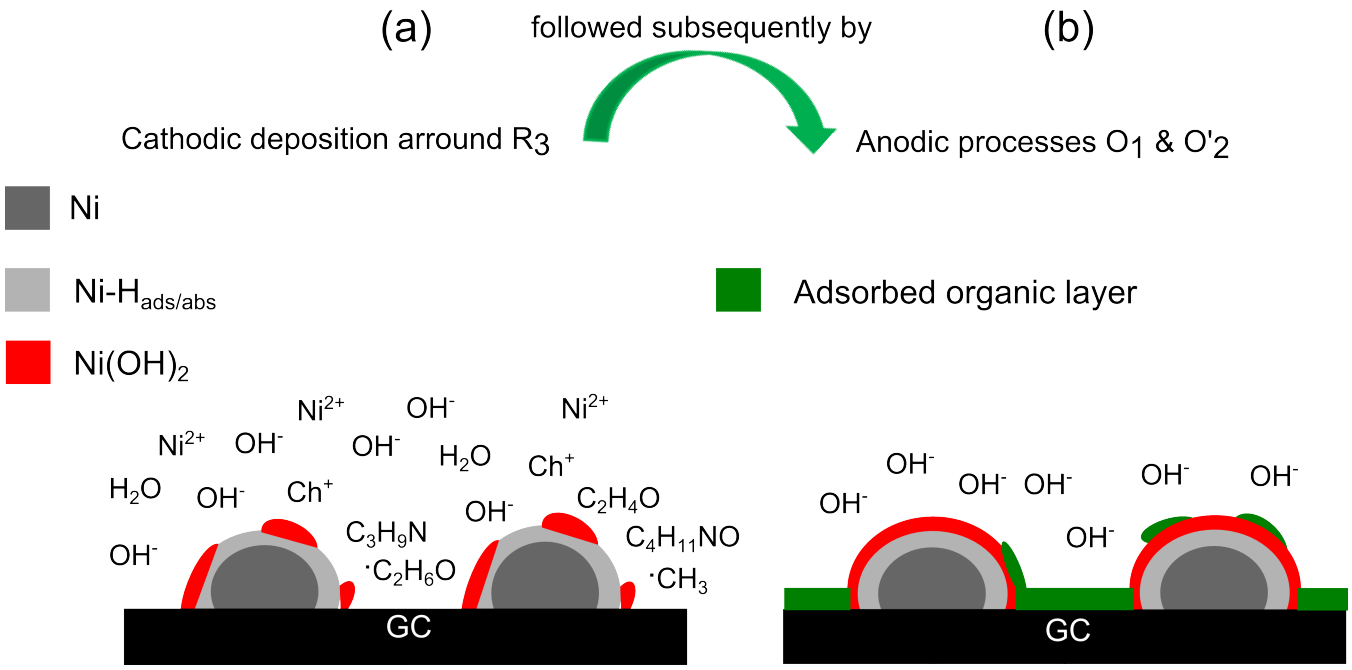

Figure 12: Scheme of the Ni NPs (a) deposited at highly negative potential ($E = -1.1$ V) and (b) after the anodic processes O_1 and O'_2

can be of great interest for their electrocatalytic activity for different processes, such as the oxygen evolution reaction (OER). Therefore, a detailed study on the formation mechanism of these structures and their activity for OER are deeply detailed in a follow up publication.

Conclusions

The electrodeposition of nickel nanostructures on glassy carbon was investigated in 1:2 choline chloride urea (1:2 ChCl-U) DES containing different amounts of water. By combining electrochemical techniques with ex-situ FE-SEM, HAADF-STEM and EDX, the electrochemical processes occurring during nickel deposition and the effect of water content were better understood. At highly negative potentials, Ni growth is halted due to water splitting and the formation of a mixed layer of $Ni/NiO_x(OH)_{2(1-x)}$. Moreover, under certain conditions, the DES components can also be (electro)chemically reduced at the electrode surface, blocking further 3D growth of the Ni NPs. Hence, a 2D crystalline Ni network can be formed

in the inter-particle region. Careful tuning of the water content leads to a fine control of the deposition potentials of Ni and the side reactions occurring at more negative potentials, giving the ability to control self-limiting growth and passivation phenomena.

Supporting Information Available

Water content. The 3^{rd} scan of the CVs of Figures 1, 2 and 3. Influence of stirring. Selected area electron diffraction (SAED).

Acknowledgements

E.A. Mernissi Cherigui and Mesfin Haile Mamme acknowledge funding from the Fonds Wetenschappelijk Onderzoek in Flanders (FWO, research project G019014N). S. Bals acknowledges funding from the European Research Council (Starting Grant No. COLOURATOMS 335078). Finally, J. Ustarroz acknowledges funding from the Fonds Wetenschappelijk Onderzoek in Flanders (FWO, postdoctoral grant 12I7816N).

References

(1) Li, G.-R.; Xu, H.; Lu, X.-F.; Feng, J.-X.; Tong, Y.-X.; Su, C.-Y. Electrochemical synthesis of nanostructured materials for electrochemical energy conversion and storage. *Nanoscale* **2013**, *5*, 4056–4069.

(2) Wei, L.; Fan, Y.-J.; Wang, H.-H.; Tian, N.; Zhou, Z.-Y.; Sun, S.-G. Electrochemically shape-controlled synthesis in deep eutectic solvents of Pt nanoflowers with enhanced activity for ethanol oxidation. *Electrochim. Acta* **2012**, *76*, 468–474.

(3) Gómez, E.; Pollina, R.; Vallés, E. Nickel electrodeposition on different metallic substrates. *J. Electroanal. Chem.* **1995**, *386*, 45–56.

(4) Proud, W. G.; Gomez, E.; Sarret, E.; Valles, E.; Müller, C. Influence of pH on nickel electrodeposition at low nickel(II) concentrations. *J. Appl. Electrochem.* **1995**, *25*, 770–775.

(5) Vanpaemel, J.; van der Veen, M. H.; De Gendt, S.; Vereecken, P. M. Enhanced nucleation of Ni nanoparticles on TiN through H3BO3-mediated growth inhibition. *Electrochim. Acta* **2013**, *109*, 411–418.

(6) Vanpaemel, J.; Sugiura, M.; Cuypers, D.; Van Der Veen, M. H.; De Gendt, S.; Vereecken, P. M. Electrochemical deposition of subnanometer Ni films on TiN. *Langmuir* **2014**, *30*, 2047–2053.

(7) Cheng, Q.; Wu, C.; Chen, J.; Zhou, Y.; Wu, K. Electrochemical tuning the activity of nickel nanoparticle and application in sensitive detection of chemical oxygen demand. *J. Phys. Chem. C* **2011**, *115*, 22845–22850.

(8) Bayandori Moghaddam, A.; Ganjali, M. R.; Saboury, A. A.; Moosavi-Movahedi, A. A.; Norouzi, P. Electrodeposition of nickel oxide nanoparticles on glassy carbon surfaces: application to the direct electron transfer of tyrosinase. *J. Appl. Electrochem.* **2008**, *38*, 1233–1239.

(9) Jin, C.; Zeng, A.; Cho, S. J.; Nam, S. H.; Seo, H. O.; Kim, Y. D.; Boo, J. H. Effect of deposition time and potential on the nucleation and growth of nickel nano particles on nitrogen doped diamond-like carbon thin film. *Thin Solid Films* **2012**, *521*, 158–162.

(10) Salimi, A.; Sharifi, E.; Noorbakhsh, A.; Soltanian, S. Direct voltammetry and electrocatalytic properties of hemoglobin immobilized on a glassy carbon electrode modified with nickel oxide nanoparticles. *Electrochem. commun.* **2006**, *8*, 1499–1508.

(11) Salimi, A.; Sharifi, E.; Noorbakhsh, A.; Soltanian, S. Immobilization of glucose oxidase on electrodeposited nickel oxide nanoparticles: Direct electron transfer and electrocatalytic activity. *Biosens. Bioelectron.* **2007**, *22*, 3146–3153.

(12) Chelaghmia, M. L.; Nacef, M.; Affoune, A. M. Ethanol electrooxidation on activated graphite supported platinum-nickel in alkaline medium. *J. Appl. Electrochem.* **2012**, *42*, 819–826.

(13) Schlesinger, M.; Paunovic, M. *Modern Electroplating*; Wiley: Hoboken, NJ, 2010.

(14) Smith, E. L.; Abbott, A. P.; Ryder, K. S. Deep Eutectic Solvents (DESs) and Their Applications. *Chem. Rev.* **2014**, *114*, 11060–11082.

(15) Wagle, D. V.; Zhao, H.; Baker, G. A. Deep Eutectic Solvents: Sustainable Media for Nanoscale and Functional Materials. *Acc. Chem. Res.* **2014**, *47*, 2299–2308.

(16) Bund, A.; Zschippang, E. Nickel Electrodeposition from a Room Temperature Eutectic Melt. *ECS Trans.* **2007**, *3*, 253–261.

(17) Abbott, a. P.; El Ttaib, K.; Ryder, K. S.; Smith, E. L. Electrodeposition of nickel using eutectic based ionic liquids. *Trans. IMF* **2008**, *86*, 234–240.

(18) Abbott, A. P.; Ballantyne, A.; Harris, R. C.; Juma, J. A.; Ryder, K. S. Bright metal coatings from sustainable electrolytes: the effect of molecular additives on electrodeposition of nickel from a deep eutectic solvent. *Phys. Chem. Chem. Phys.* **2017**, *19*, 3219–3231.

(19) Rostom Ali, M.; Rahman, M. Z.; Sankar Saha, S. Electroless and electrolytic deposition of nickel from deep eutectic solvents based on choline chloride. *Indian J. Chem. Technol.* **2014**, *21*, 127–133.

(20) Yang, H.; Guo, X.; Birbilis, N.; Wu, G.; Ding, W. Tailoring nickel coatings via electrodeposition from a eutectic-based ionic liquid doped with nicotinic acid. *Appl. Surf. Sci.* **2011**, *257*, 9094–9102.

(21) Yang, H. Y.; Guo, X. W.; Chen, X. B.; Wang, S. H.; Wu, G. H.; Ding, W. J.; Birbilis, N.

On the electrodeposition of nickel-zinc alloys from a eutectic-based ionic liquid. *Electrochim. Acta* **2012**, *63*, 131–138.

(22) Srivastava, M.; Yoganandan, G.; Grips, V. K. W. Electrodeposition of Ni and Co coatings from ionic liquid. *Surf. Eng.* **2012**, *28*, 424–429.

(23) Cai, G.; Gu, C.; Zhang, J.; Liu, P.; Wang, X.; You, Y.; Tu, J. Ultra fast electrochromic switching of nanostructured NiO films electrodeposited from choline chloride-based ionic liquid. *Electrochim. Acta* **2013**, *87*, 341–347.

(24) Costovici, S.; Manea, A.-C.; Visan, T.; Anicai, L. Investigation of Ni-Mo and Co-Mo alloys electrodeposition involving choline chloride based ionic liquids. *Electrochim. Acta* **2016**, *207*, 97–111.

(25) You, Y.; Gu, C.; Wang, X.; Tu, J. Electrodeposition of NiCo alloys from a deep eutectic solvent. *Surf. Coatings Technol.* **2012**, *206*, 3632–3638.

(26) Bernasconi, R.; Magagnin, L. Electrodeposition of nickel from DES on aluminium for corrosion protection. *Surf. Eng.* **2017**, *33*, 131–135.

(27) Wang, S.; Guo, X.; Yang, H.; Dai, J.; Zhu, R.; Gong, J.; Peng, L.; Ding, W. Electrodeposition mechanism and characterization of Ni-Cu alloy coatings from a eutectic-based ionic liquid. *Appl. Surf. Sci.* **2014**, *288*, 530–536.

(28) Florea, A.; Anicai, L.; Costovici, S.; Golgovici, F.; Visan, T. Ni and Ni alloy coatings electrodeposited from choline chloride-based ionic liquids - Electrochemical synthesis and characterization. *Surf. Interface Anal.* **2010**, *42*, 1271–1275.

(29) Gu, C.; You, Y.; Yu, Y.; Qu, S.; Tu, J. Microstructure, nanoindentation, and electrochemical properties of the nanocrystalline nickel film electrodeposited from choline chlorideethylene glycol. *Surf. Coatings Technol.* **2011**, *205*, 4928–4933.

(30) Gu, C.; Tu, J. One-Step Fabrication of Nanostructured Ni Film with Lotus Effect from Deep Eutectic Solvent. *Langmuir* **2011**, *27*, 10132–10140.

(31) Abbott, A. P.; Ballantyne, A.; Harris, R. C.; Juma, J. A.; Ryder, K. S.; Forrest, G. A Comparative Study of Nickel Electrodeposition Using Deep Eutectic Solvents and Aqueous Solutions. *Electrochim. Acta* **2015**, *176*, 718–726.

(32) Aldana-González, J.; Romero-Romo, M.; Robles-Peralta, J.; Morales-Gil, P.; Palacios-González, E.; Ramírez-Silva, M.; Mostany, J.; Palomar-Pardavé, M. On the electrochemical formation of nickel nanoparticles onto glassy carbon from a deep eutectic solvent. *Electrochim. Acta* **2018**, *276*, 417–423.

(33) Sebastian, P.; Giannotti, M. I.; Gómez, E.; Feliu, J. M. Surface Sensitive Nickel Electrodeposition in Deep Eutectic Solvent. *ACS Appl. Energy Mater.* **2018**, *1*, 1016–1028.

(34) Wang, S.; Zou, X.; Lu, Y.; Rao, S.; Xie, X.; Pang, Z.; Lu, X.; Xu, Q.; Zhou, Z. Electrodeposition of nano-nickel in deep eutectic solvents for hydrogen evolution reaction in alkaline solution. *Int. J. Hydrogen Energy* **2018**, 1–14.

(35) Yanai, T.; Yamaguchi, T.; Akiyoshi, T.; Takashima, K.; Nakano, M.; Fukunaga, H. Effects of Glycine in DES-Based Plating Baths on Structural and Magnetic Properties of FeNi Films. *IEEE Trans. Magn.* **2017**, *53*, 1–4.

(36) Hammons, J. A.; Muselle, T.; Ustarroz, J.; Tzedaki, M.; Raes, M.; Hubin, A.; Terryn, H. Stability, assembly, and particle/solvent interactions of Pd nanoparticles electrodeposited from a deep eutectic solvent. *J. Phys. Chem. C* **2013**, *117*, 14381–14389.

(37) Mahyari, F. A.; Tohidi, M.; Safavi, A. Synthesis of gold nanoflowers using deep eutectic solvent with high surface enhanced Raman scattering properties. *Mater. Res. Express* **2016**, *3*, 095006.

(38) Lee, J.-S. Deep eutectic solvents as versatile media for the synthesis of noble metal nanomaterials. *Nanotechnol. Rev.* **2017**, *6*, 271–278.

(39) Mernissi Cherigui, E. A.; Sentosun, K.; Bouckenooge, P.; Vanrompay, H.; Bals, S.; Terryn, H.; Ustarroz, J. Comprehensive Study of the Electrodeposition of Nickel Nanostructures from Deep Eutectic Solvents: Self-Limiting Growth by Electrolysis of Residual Water. *J. Phys. Chem. C* **2017**, *121*, 9337–9347.

(40) Wang, R.; Bertocci, U.; Tan, H.; Bendersky, L. A.; Moffat, T. P. Self-Terminated Electrodeposition of Ni, Co and Fe Ultrathin Films. *J. Phys. Chem. C* **2016**, *120*, 16228–16237.

(41) Ritzert, N. L.; Moffat, T. P. Ultramicroelectrode Studies of Self-Terminated Nickel Electrodeposition and Nickel Hydroxide Formation upon Water Reduction. *J. Phys. Chem. C* **2016**, *120*, 27478–27489.

(42) Shah, D.; Mjalli, F. S. Effect of water on the thermo-physical properties of Reline: An experimental and molecular simulation based approach. *Phys. Chem. Chem. Phys.* **2014**, *16*, 23900–23907.

(43) Passos, H.; Tavares, D. J. P.; Ferreira, A. M.; Freire, M. G.; Coutinho, J. A. P. Are Aqueous Biphasic Systems Composed of Deep Eutectic Solvents Ternary or Quaternary Systems? *ACS Sustain. Chem. Eng.* **2016**, *4*, 2881–2886.

(44) Hammond, O. S.; Bowron, D. T.; Edler, K. J. The Effect of Water upon Deep Eutectic Solvent Nanostructure: An Unusual Transition from Ionic Mixture to Aqueous Solution. *Angew. Chemie - Int. Ed.* **2017**, *56*, 9782–9785.

(45) Grishina, E. P.; Kudryakova, N. O. Conductivity and electrochemical stability of concentrated aqueous choline chloride solutions. *Russ. J. Phys. Chem. A* **2017**, *91*, 2024–2028.

(46) Meng, X.; Ballerat-Busserolles, K.; Husson, P.; Andanson, J.-M. Impact of water on the melting temperature of urea + choline chloride deep eutectic solvent. *New J. Chem.* **2016**, *40*, 4492–4499.

(47) D'Agostino, C.; Gladden, L. F.; Mantle, M. D.; Abbott, A. P.; Ahmed, I., Essa; Al-Murshedi, A. Y. M.; Harris, R. C. Molecular and ionic diffusion in aqueous deep eutectic solvent mixtures: probing inter-molecular interactions using PFG NMR. *Phys. Chem. Chem. Phys.* **2015**, *17*, 15297–15304.

(48) Pandey, A.; Rai, R.; Pal, M.; Pandey, S. How polar are choline chloride-based deep eutectic solvents? *Phys. Chem. Chem. Phys.* **2014**, *16*, 1559–1568.

(49) Florindo, C.; Oliveira, F. S.; Rebelo, L. P.; Fernandes, A. M.; Marrucho, I. M. Insights into the synthesis and properties of deep eutectic solvents based on cholinium chloride and carboxylic acids. *ACS Sustain. Chem. Eng.* **2014**, *2*, 2416–2425.

(50) Protsenko, V.; Kityk, A.; Shaiderov, D.; Danilov, F. Effect of water content on physicochemical properties and electrochemical behavior of ionic liquids containing choline chloride, ethylene glycol and hydrated nickel chloride. *J. Mol. Liq.* **2015**, *212*, 716–722.

(51) Du, C.; Zhao, B.; Chen, X.-b.; Birbilis, N.; Yang, H. Effect of water presence on choline chloride-2urea ionic liquid and coating platings from the hydrated ionic liquid. *Sci. Rep.* **2016**, *6*, 29225.

(52) Oh, J.-H.; Lee, J.-S. Synthesis of Gold Microstructures with Surface Nanoroughness Using a Deep Eutectic Solvent for Catalytic and Diagnostic Applications. *J. Nanosci. Nanotechnol.* **2014**, *14*, 3753–3757.

(53) Ustarroz, J.; Gupta, U.; Hubin, A.; Bals, S.; Terryn, H. Electrodeposition of Ag nanoparticles onto carbon coated TEM grids: A direct approach to study early stages of nucleation. *Electrochem. commun.* **2010**, *12*, 1706–1709.

(54) Ustarroz, J.; Altantzis, T.; Hammons, J. a.; Hubin, A.; Bals, S.; Terryn, H. The Role of Nanocluster Aggregation, Coalescence, and Recrystallization in the Electrochemical Deposition of Platinum Nanostructures. *Chem. Mater.* **2014**, *26*, 2396–2406.

(55) Oshchepkov, A. G.; Bonnefont, A.; Saveleva, V. A.; Papaefthimiou, V.; Zafeiratos, S.; Pronkin, S. N.; Parmon, V. N.; Savinova, E. R. Exploring the Influence of the Nickel Oxide Species on the Kinetics of Hydrogen Electrode Reactions in Alkaline Media. *Top. Catal.* **2016**, *59*, 1319–1331.

(56) Haerens, K.; Matthijs, E.; Binnemans, K.; Van der Bruggen, B. Electrochemical decomposition of choline chloride based ionic liquid analogues. *Green Chem.* **2009**, *11*, 1357–1365.

(57) Weininger, J. L.; Breiter, M. W. Hydrogen Evolution and Surface Oxidation of Nickel Electrodes in Alkaline Solution. *J. Electrochem. Soc.* **1964**, *111*, 707–712.

(58) Floner, D.; Lamy, C.; Leger, J. M. Electrocatalytic oxidation of hydrogen on polycrystal and single-crystal nickel electrodes. *Surf. Sci.* **1990**, *234*, 87–97.

(59) Machado, S. A.; Avaca, L. A. The hydrogen evolution reaction on nickel surfaces stabilized by H-absorption. *Electrochim. Acta* **1994**, *39*, 1385–1391.

(60) Visscher, W.; Barendrecht, E. Absorption of hydrogen in reduced nickel oxide. *J. Appl. Electrochem.* **1980**, *10*, 269–274.

(61) Vecchi, L.; Simillion, H.; Montoya, R.; Laethem, D. V.; Eeckhout, E. V. D.; Verbeken, K.; Terryn, H.; Deconinck, J.; Ingelgem, Y. V. Electrochimica Acta Modelling of hydrogen permeation experiments in iron alloys : Characterization of the accessible parameters e Part II e The exit side. *Electrochimica Acta* **2018**, *262*, 153–161.

(62) Hall, D. S.; Bock, C.; Macdougall, B. R. The Electrochemistry of Metallic Nickel :

Oxides , Hydroxides , Hydrides and Alkaline Hydrogen Evolution. *J. Electrochem. Soc.* **2013**, *160*, 235–243.

(63) Oshchepkov, A. G.; Bonnefont, A.; Parmon, V. N.; Savinova, E. R. On the effect of temperature and surface oxidation on the kinetics of hydrogen electrode reactions on nickel in alkaline media. *Electrochim. Acta* **2018**, *269*, 111–118.

(64) Sebastián, P.; Botello, L. E.; Vallés, E.; Gómez, E.; Palomar-Pardavé, M.; Scharifker, B. R.; Mostany, J. Three-dimensional nucleation with diffusion controlled growth: A comparative study of electrochemical phase formation from aqueous and deep eutectic solvents. *J. Electroanal. Chem.* **2017**, *793*, 119–125.

(65) Haile Mamme, M. Early stages of electrochemical growth of nanoparticles, new insights through multiscale modelling. Ph.D. thesis, Vrije Universiteit Brussel, 2018.

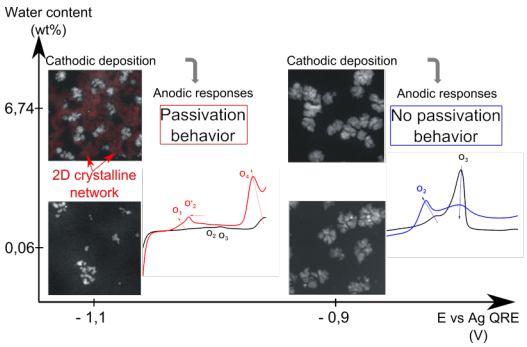
Water content
(wt%)
6,74
0,06
Cathodic deposition
Anodic responses
Passivation
behavior
2D crystalline
network
Cathodic deposition
Anodic responses
No passivation
behavior
- 1,1
- 0,9
E vs Ag QRE
(V)

TOC Graphic